Biomed Microdevices (2006) 8:299–308
DOI 10.1007/s10544-006-0033-0

Combined microfluidic-micromagnetic separation of living cells in continuous flow

Nan Xia · Tom P. Hunt · Brian T. Mayers · Eben Alsberg · George M. Whitesides · Robert M. Westervelt · Donald E. Ingber

Published online: 25 September 2006

Abstract This paper describes a miniaturized, integrated, microfluidic device that can pull molecules and living cells bound to magnetic particles from one laminar flow path to another by applying a local magnetic field gradient, and thus selectively remove them from flowing biological fluids without any wash steps. To accomplish this, a microfabricated high-gradient magnetic field concentrator (HGMC) was integrated at one side of a microfluidic channel with two inlets and outlets. When magnetic micro- or nano-particles were introduced into one flow path, they remained limited to that flow stream. In contrast, when the HGMC was magnetized, the magnetic beads were efficiently pulled from the initial flow path into the collection stream, thereby cleansing the original fluid. Using this microdevice, living *E. coli* bacteria bound to magnetic nanoparticles were efficiently removed from flowing solutions containing densities of red blood cells similar to that found in blood. Because this microdevice allows large numbers of beads and cells to be sorted simultaneously, has no capacity limit, and does not lose separation efficiency as particles are removed, it may be especially useful for separations from blood or other clinical samples. This on-chip HGMC-microfluidic separator technology may potentially allow cell separations to be carried out in the field outside of hospitals and clinical laboratories.

Keywords Nanotechnology · Bioseparations · Microfluidics · Magnetic particles · Bacteria · Magnetic field gradient concentrator

N. Xia · E. Alsberg · D. E. Ingber (✉)
Vascular Biology Program, Departments of Pathology & Surgery, Karp Family Research Laboratories, Children's Hospital and Harvard Medical School, Boston, MA 02115, USA
e-mail: donald.ingber@childrens.harvard.edu

E. Alsberg
Present address: Department of Biomedical Engineering, Case Western Reserve University, Cleveland, OH 44106, USA

T. P. Hunt · R. M. Westervelt
Department of Physics and Division of Engineering and Applied Sciences, Harvard University, Cambridge, MA 02138, USA

B. T. Mayers · G. M. Whitesides
Department of Chemistry and Chemical Biology, Harvard University, Cambridge, MA 02138, USA

Introduction

One of the key functions required for microsystems technologies used for biomedical applications is to separate specific cells or molecules from complex biological mixtures, such as blood, urine or cerebrospinal fluid. Various physical properties, including size (Huang et al., 2004; Yamada et al., 2004), motility (Cho et al., 2003), electric charge (Lu et al., 2004), electric dipole moment (Fiedler et al., 1998; Hunt et al., 2004), and optical qualities (Fu et al., 1999; Wang et al., 2005), have been exploited for this purpose. Magnetic susceptibility also has been explored (Pamme, 2006) because magnetic sorting can be carried out at high-throughput in virtually any biological fluid with minimal power requirements, and without damaging the sorted entities (Franzreb et al., 2006; Hirschbein et al., 1982; Lee et al., 2004; Safarik and Safarikova, 1999; Setchell, 1985). Biocompatible superparamagnetic particles are also now widely available with surfaces modified to promote binding to various molecules and cells. In fact, various macroscale magnetic sorting systems have been built and employed for research and clinical applications (Chalmers et al., 1998; Fuh and Chen, 1998; Handgretinger et al., 1998; Hartig et al., 1995; Melville et al., 1975a; Takayasu et al., 2000) (e.g. to isolate stem cells from

batches of pooled blood for bone marrow reconstitution procedures in cancer patients (Handgretinger et al., 1998)).

Batch-type magnetic separators have been microfabricated on single chips that trap magnetic particles in flowing fluids using an external magnetic field, and then the particles are later eluted from the system (Ahn et al., 1996; Deng et al., 2002; Smistrup et al., 2005; Tibbe et al., 2002). But the loading capacity of these devices is limited because accumulation of the collected particles can restrict fluid flow or lead to irreversible entrapment of samples, and their use is hampered by the need to disrupt continuous operation for sample elution.

Continuous on-chip separation could greatly simplify microsystem operation, and potentially improve separation efficiency. In particular, microfluidic systems that are extensively utilized in micro-total analysis systems (μTAS) offer the potential to separate components continuously from flowing liquids. Continuous separation of magnetic particles in microfluidic channels has been demonstrated by manually placing a permanent magnet or electromagnet beside a microchannel that contains multiple outlets (Blankenstein, 1997; Kim and Park, 2005; Pamme and Manz, 2004). However, because each magnet needs to be individually fabricated and positioned, further miniaturization and multiplexing is not possible with this approach.

High-gradient magnetic concentrators (HGMCs) can generate a large magnetic force with simple device structures. Macroscale HGMCs have been used in magnetic separations for biomedical applications (Chalmers et al., 1998; Fuh and Chen, 1998; Hartig et al., 1995; Melville et al., 1975a; Takayasu et al., 2000), but are impractical for microsystems technologies due to their large dimensions. With the development of microfabrication technologies, it has become possible to microfabricate HGMCs along with microfluidic channels on a single chip. Several on-chip HGMC-microfluidic designs for continuous magnetic separation have been reported (Berger et al., 2001; Han and Frazier, 2004, 2006; Inglis et al., 2004). One design used microfabricated magnetic stripes aligned on the bottom of the fluid chamber to horizontally separate magnetically tagged leukocytes trapped on the magnetic stripes away from red blood cells (RBCs) flowing through the chamber (Inglis et al., 2004). In another design, a microfabricated magnetic wire was placed in the middle of the flow stream along the length of a single microfluidic channel, and used to separate deoxyhemoglobin RBCs from white blood cells based on the difference in their relative magnetic susceptibilities (Han and Frazier, 2006).

Our laboratory is interested in developing on-chip technologies for magnetic separation of living cells from biological fluids (e.g., blood, cerebrospinal fluid) which could be potentially used to develop portable devices for in-field diagnosis or therapy of diseases caused by blood-born pathogens, such as sepsis. If effective, this same type of on-chip magnetic separation technologies may also be potentially useful for isolating rare cells, such as cancer cells, stem cells or fetal cells in the maternal circulation. For these goals, it was necessary to develop a new on-chip HGMC-microfluidic approach that offers improvements over the existing designs in terms of biocompatibility, separation efficiency, and rate of clearance, while minimizing the disturbance on normal blood cells and biomolecules. Here we describe a novel microfabricated on-chip HGMC-microfluidic system that permits efficient separation of magnetic micro- and nano-particles, either alone or bound to living bacteria, under continuous fluid flow.

Experimental

Microsystem fabrication

The microfluidic channel was prepared by soft lithography (McDonald and Whitesides, 2002) and has dimensions of $20 \times 0.2 \times 0.05$ mm (L $\times$ W $\times$ H). A negative mold of the channel was produced in SU-8 photoresist (Microchem, Inc.). Poly(dimethylsiloxane) (PDMS) (Slygard 184, Dow Corning) was poured onto the mold, allowed to cure for 1 hour at 65°C, and peeled off. A lift-off process (Wolf, 1986) was used to define a base layer of evaporated metal (Ti/Au, 10 nm/50 nm) in the form of a microneedle (20 mm in X, 100 μm in Y, 50 μm in Z) or microcomb (3.8 mm in X, 12 mm in Y, 50 μm in Z with teeth 300 μm in X and spaced by 200 μm in Y) on a glass substrate that was then electroplated (1 mA for 4 hr) with a 50 μm thick layer of magnetic material (80% Ni, 20% Fe), as previously described (Rasmussen et al., 2001). The PDMS channel and the glass substrate with the NiFe layer were exposed to oxygen plasma (100 W, 60 sec) and bonded together.

Beads and cells

Non-magnetic red-fluorescent beads (2 μm diameter, 4.5×10^9 beads/ml, Molecular Probes) and superparamagnetic green-fluorescent beads (1.6 μm, 43% iron oxide, 3.1×10^9 beads/ml, Bangs Laboratories) were incubated in 10 $\times$ volume of 1% albumin solution for 1 hour before being combined and injected into the microfluidic channel *E. coli* (HB101 K-12) bacteria expressing green fluorescent protein (GFP) were grown overnight at 37°C in LB medium containing ampicillin (100 μg/ml) and arabinose (0.1%, inductor of GFP expression), then harvested and resuspended in PBS buffer. The *E. coli* (1×10^9 CFU/ml) were labeled with biotinylated anti-E. coli antibody (Virostat; mixing ratio 2 μg antibody/10^7 cells), and mixed with streptavidin-coated superparamagnetic particles (130 nm, 85% iron oxide, G.Kisker GbR) prior addition to the

microfluidic system. Human RBCs (75% hematocrit) were obtained from the blood bank at Children's Hospital Boston, stained with the red fluorescent dye (SYTO 64, Molecular Probes), and mixed with isotonic saline containing 0.5% albumin at a 1:3 ratio (final density around 2×10^9 RBCs/ ml).

Microfluidic control

Fluidic connections to the microfluidic channel were made with polyethylene tubing inserted through holes punched through the PDMS. Syringe pumps were used to control the flow rate at each of the inlet independently. Prior to each experiment, the flow channel and tubing were cleaned by flushing with 70% ethanol, rinsing with deionized water, and incubating in phosphate buffered saline (PBS) with 1% albumin for 30 min. The fluid containing the sample and a dextran solution (32%, 70 kDa) were injected simultaneously into the source and collection inlets, respectively. All experiments were carried out using experimental samples contained within the first half of the volume from syringes in the upright position. Separations of particles and cells in the microchannel were monitored in real-time using an inverted Nikon TE2000-E microscope equipped with a CCD camera, and optimized by adjusting the flow rate and the output split ratio. The width of the source stream was maintained as 1/3–1/2 of the channel width. A disk-shaped (4 mm diameter, 2 mm high, magnetized along the z-axis) neodymium permanent magnet was used to magnetize the NiFe layer. It was positioned in the middle of the NiFe layer in the flow direction with its center 4 to 5 mm from the closest side of the microfluidic channel using a microscope micromanipulator.

Quantification of separation efficiencies

Quantification of clearance efficiency using the fluorescent microbeads was performed using the inverted Nikon TE2000-E microscope by measuring the fluorescence intensity of the collected fluids from both outlets. In studies with *E. coli*, the high density of bound magnetic nanoparticles blocked the GFP signal. Thus, bacterial numbers were quantified by transferring the fluids collected from the outlets to growth medium and culturing at 37°C. The optical density of the cell solutions at 600 nm ($OD_{600\,nm}$) was measured periodically. Cell numbers were estimated using $OD_{600\,nm}$ obtained during the logarithmic phase of growth; we confirmed that $OD_{600\,nm}$ during this phase was linearly related to the starting concentration of the magnetically-labeled *E. coli* bacteria.

Results

Figure 1 shows a schematic illustration of the design of our prototype, on-chip HGMC-microfluidic separator. In this design, a single microfluidic channel is connected to two inlets and two outlets. Due to the small Reynolds number (Re) of microfluidic channels, the flow remains laminar with mixing due only to diffusion across the streamlines. A layer of magnetic material (NiFe) with the same thickness as the height of the microfluidic channel was deposited adjacent to the channel during the microfabrication process to create an on-chip HGMC with defined geometry (e.g., needle or comb). When magnetized by an external permanent neodymium magnet, the HGMC can locally concentrate the gradient of the applied magnetic field to pull the magnetic particles that are present in the source flow path (upper path in Fig. 1 inset) across the laminar flow streamlines and into the neighboring collection flow stream (lower path in Fig. 1 inset); these particles will then exit through the lower collection outlet. Under the same conditions, non-magnetic particles in the source flow path should be unaffected by the applied magnetic field gradient, and thus, they will exit through the upper source outlet.

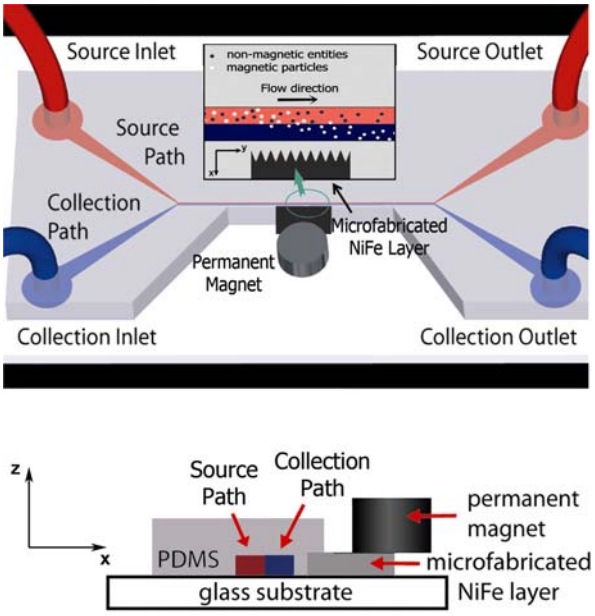

Fig. 1 Schematic depiction of the combined micromagnetic-microfluidic separation device that contains a microfabricated layer of soft magnetic NiFe material adjacent to a microfluidic channel with two inlets and outlets; both 3D (top) and cross-sectional (bottom) views of the microdevice are illustrated. Inset shows how magnetic beads flowing in the upper source path are pulled across the laminar streamline boundary into the lower collection path when subjected to a magnetic field gradient produced by the microfabricated NiFe layer located along the lower side of the channel. In our system, the fluid flow is in the y-direction, the magnetic field gradient across the channel is in the x-direction, and the channel height is in the z-direction

Initial studies carried out in the absence of an HGMC (NiFe layer) revealed that at a volume flow rate of 5 μl/hr (0.3 mm/s), the external neodymium magnet alone was not sufficient to pull magnetic beads (1.6 μm diameter) flowing in PBS across the boundary between adjacent laminar streams (Fig. 2(A)). Computer simulations (Maxwell 3D,

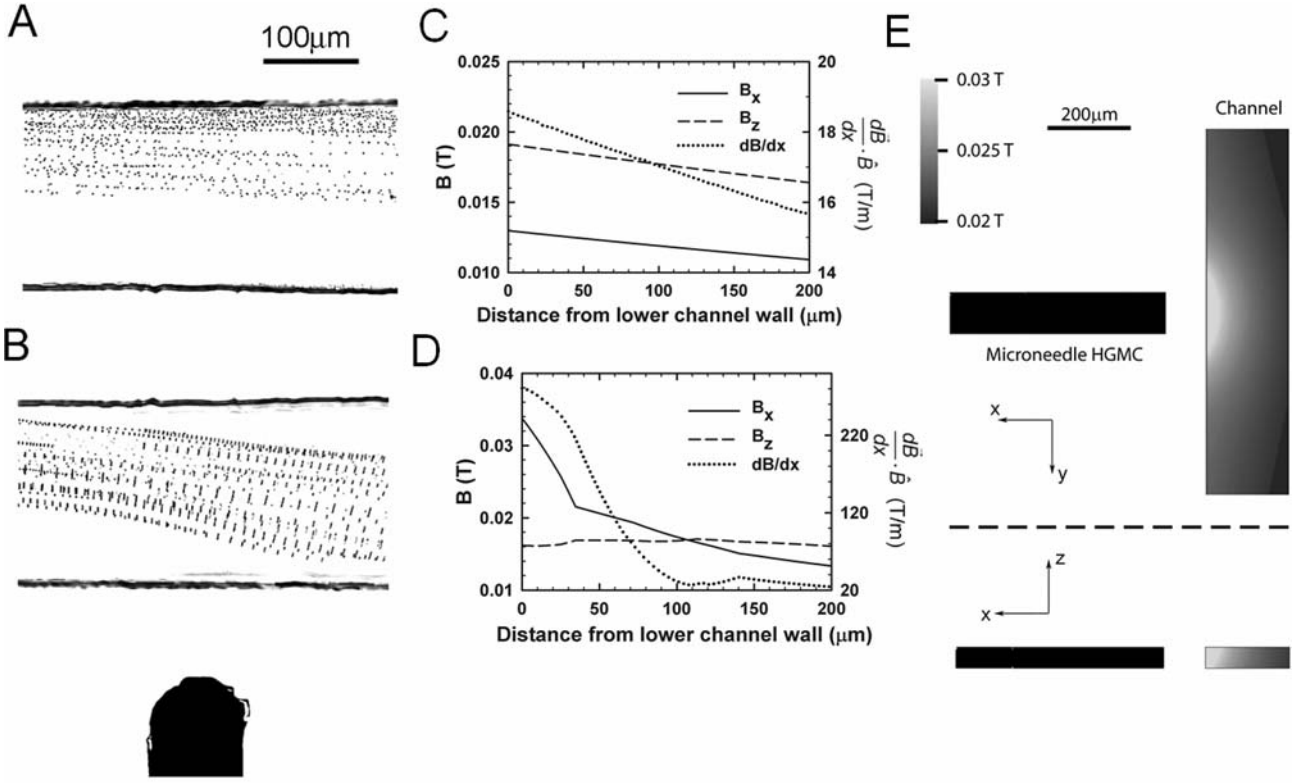

Fig. 2 Bright field microscopic images of the flow pattern of 1.6 μm magnetic beads in the microfluidic channel in the absence (A) or presence (B) of the microfabricated NiFe microneedle when a magnetic field is applied using a neodymium disk magnet. The images are constructed by overlaying sequential frames of the corresponding time-lapse movies recorded at the middle of the channel. The corresponding magnetic field and magnetic field gradient are presented as a function of distance from the lower (collection stream side) channel wall in (C) and (D), respectively. The solid, dashed and dotted lines correspond to the vertical magnetic field (B_z), horizontal magnetic field (B_x) and the magnetic field gradient across the channel ($\frac{d\vec{B}}{dx} \cdot \hat{B}$), respectively. (E) Computer-simulated magnetic field distributions depicted as grayscale variations within the microfluidic channel generated by the magnetized NiFe microneedle. Both top (top) and cross-sectional (bottom) views are illustrated

Ansoft; see Appendix) revealed that this configuration generated a magnetic field gradient of 15 T/m in the channel, and produced a field less than 0.02 T even at the bottom edge of the lower flow path (Fig. 2(C)). In contrast, at the same flow rate, the microfabricated device containing a magnetized NiFe HGMC in the form of a microneedle oriented perpendicularly to the flow path and juxtaposed to the side of the microfluidic channel was able to drive the magnetic beads flowing in the upper source path to cross over the streamline boundary and enter the lower path (Fig. 2(B)), eventually exiting through the collection outlet. This separation was made possible because the NiFe microneedle generated a stronger magnetic field gradient across the channel (>25 T/m), with a field strength in the vertical and horizontal directions of >0.016 and >0.013 T, respectively (Fig. 2(D) and (E); see Appendix), when magnetized by the external neodymium magnet. These results demonstrate the potential utility of this on-chip HGMC-microfluidic approach. However, the separation efficiency of the device with the microneedle shaped HGMC was low: less than 20% of the magnetic beads exited from the lower outlet at a flow rate of 25 μl/hr.

To increase the separation efficiency of the on-chip HGMC-microfluidic separator, we microfabricated the NiFe layer in a microcomb configuration that has a triangular saw-tooth edge positioned close to the side of the channel (Fig. 3(A)). Due to its high curvature geometry, the microcomb concentrates the magnetic field and produces a steep magnetic field gradient across the width of the flow channel without providing excessive trapping of particles near the channel wall. Computer simulations confirmed that the saw-tooth edge of the comb provides horizontal and vertical magnetic fields of 0.025 T and 0.018 T, respectively, at the far edge of the channel, and a field gradient of at least 50 T/m (Fig. 3(B) and (C); see Appendix). In addition, the region of the microfluidic channel exposed to the magnetic field gradient along its length (in the y-direction) was increased to 12 mm.

To analyze the performance of the micromagnetic separator with the NiFe microcomb for magnetic particle separation, green fluorescent magnetic beads (1.6 μm diameter; 1.6×10^7 beads/ml) were mixed with red fluorescent non-magnetic beads (2 μm diameter; 2.2×10^7 beads/ml) in PBS

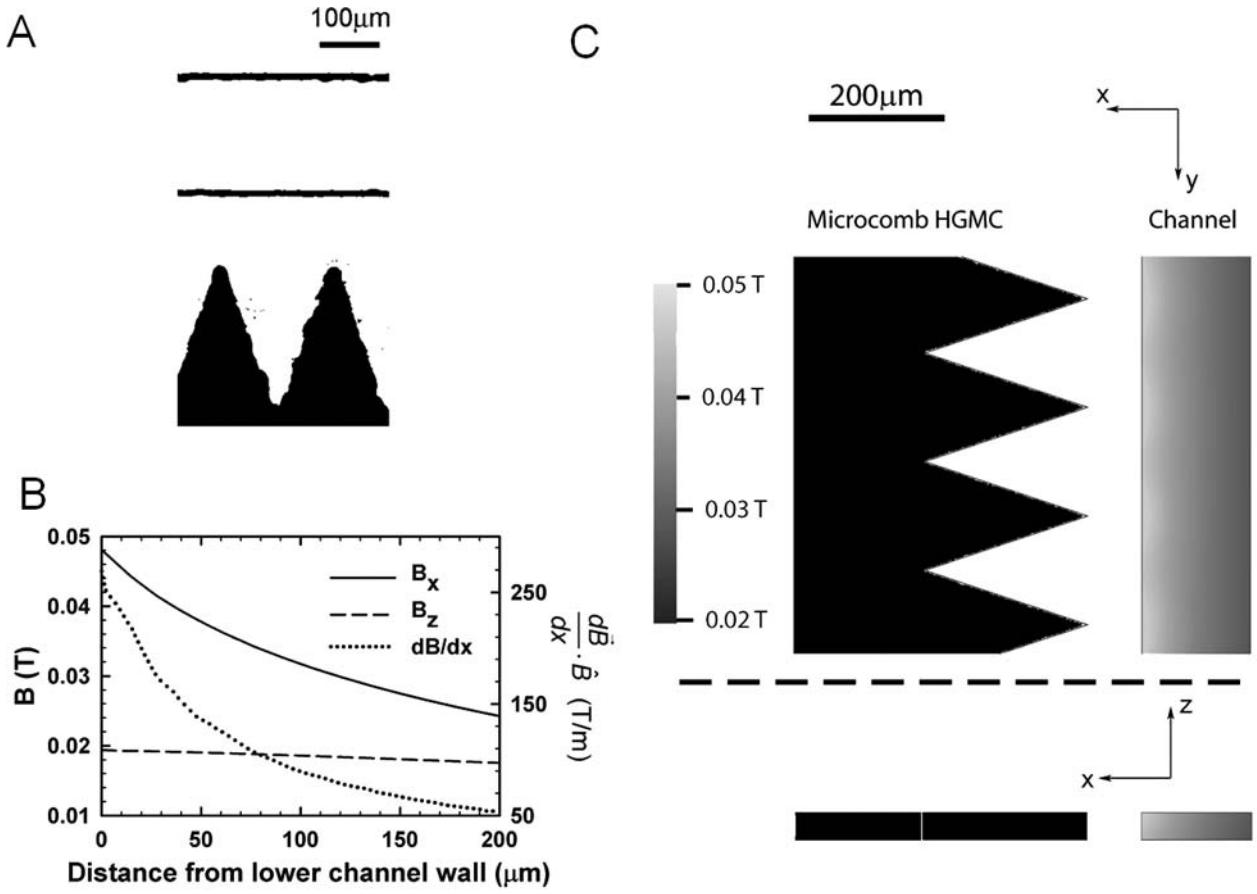

Fig. 3 (A) Microscopic view of the NiFe microcomb. (B) The corresponding magnetic field and the magnetic field gradient are presented as a function of distance from the lower (collection stream side) channel wall. The line-type assignment is the same as that in Fig. 2. (C) Computer-simulated magnetic field distributions depicted as grayscale variations within the microfluidic channel generated by the magnetized NiFe microcomb. Both top (top) and cross-sectional (bottom) views are illustrated

and introduced into the source path. Without magnetization, both the magnetic and non-magnetic beads followed their laminar flow path and thus, both the red and green microbeads exited from the top outlet (Fig. 4(A), top). When the NiFe microcomb was magnetized, almost all of the green magnetic beads observed under microscope were pulled from the source stream and exited through the lower collection outlet, whereas the red non-magnetic beads remained in the original upper flow path (Fig. 4(A), bottom).

Quantification of the separation efficiency of the magnetic beads at the collection outlet revealed that at a flow rate of 40 μl/hr, 92% of the magnetic beads exited from the collection outlet, whereas less than 1% of the non-magnetic beads were present in this fraction (Table 1). The same green magnetic beads (1.6×10^7 beads/ml) were then mixed in isotonic saline with red dye (Syto 64)-stained human RBCs at a concentration similar to that in blood (2×10^9 cells/ml), and injected into the top inlet of the microfluidic channel. Again, the magnetic beads were able to be efficiently separated from the flowing RBCs using the on-chip HGMC-microfluidic separator (Fig. 4(B), bottom vs. top). At a flow rate of 25 μl/hr, 83% of the magnetic beads and less than 1% of RBCs were retrieved from the collection outlet (Table 1). This also confirmed that the effect of the magnetic force generated by the magnetized NiFe layer on RBCs is insignificant in this system.

We then explored whether living *E. coli* bacteria could be separated from flowing fluids, either alone or when mixed with RBCs, using the on-chip HGMC-microfluidic separator. In these studies, 130 nm magnetic particles were used to label *E. coli* bacteria (1×10^7 cells/ml) by incubating the cells with biotinylated anti-*E. coli* antibody, mixing them with 130 nm magnetic nanoparticles coated with streptavidin (1.0×10^{10} particles/ml) in PBS, and then injecting them into the source inlet of the microfluidic channel. Upon activating the magnetic field gradient, almost all of the observed *E. coli* cells originally confined to the upper laminar flow path (Fig. 4(C), top) were transferred to the lower flow path and passed out through the collection outlet (Fig. 4(C), bottom). At a flow rate of 30 μl/hr, 89% the *E. coli* cells were separated from their original flow path. Similar studies confirmed that *E. coli* (5×10^6 cells/ml; 0.5×10^{10} magnetic nanoparticles/ml)

Table 1 Results of sorting particles and cells using the combined microfluidic-micromagnetic separator with the NiFe microcomb

Sample components					
Magnetic	Non-magnetic	Flow rate (μl/hr)[a]	Throughput (beads or cells/s)[b]	Separation efficiency (%)[c,d]	
1.6 μm beads	2 μm beads in PBS	40	420	92 ± 4	86 ± 6
1.6 μm beads	RBCs in saline	25	10,000	83 ± 5	79 ± 5
E. coli + 130 nm beads	PBS[e]	30	80	89 ± 6	83 ± 9
E. coli + 130 nm beads[f]	RBCs in saline	25	10,000	53 ± 8	44 ± 11
E. coli + 130 nm beads[g]	RBCs in saline	25	10,000	78 ± 10	70 ± 9

[a] The flow rate of source stream. Experiment run time was determined by the flow rate in order to collect enough fluid volume (at least 10 μl) for quantification.
[b] Throughput was estimated based on the flow rate and cell or bead density of the sample. The magnetic nanoparticles used for labeling *E. coli* were not included when calculating the throughput.
[c] The efficiency of separations carried out as shown in Fig. 4 were calculated in two ways: (Left column) $I_{c,mag}/ (I_{c,mag} + I_{s,mag})$; (Right column) $I_{c,mag}/ I_{s,non-,mag}$, where $I_{c,mag}$ and $I_{s,mag}$ are the intensity (fluorescence or $OD_{600\,nm}$) of beads or cells collected at the lower outlet and upper outlet, respectively, with magnetic field turned on, and $I_{s,non-mag}$ is the intensity (fluorescence or $OD_{600\,nm}$) of beads or cells collected at the upper outlet with magnetic field turned off.
[d] The amount of non-magnetic beads or RBCs collected at the lower outlet was less than 1% of the amount of non-magnetic beads or RBCs collected at the upper outlet in all the experiments.
[e] For better visualization of boundary of flow path, the PBS buffer contained Texas Red-conjugated bovine serum albumin (0.1 mg/ml) in this study.
[f] *E. coli* (5×10^6 cells/ml) + 130 nm magnetic particles (5×10^9 particles/ml).
[g] *E. coli* (5×10^6 cells/ml) + 130 nm magnetic particles (1.0×10^{10} particles/ml).

could be separated from saline containing a physiological concentration of RBCs (2×10^9 cells/ml), but the separation efficiency of *E. coli* at the collection outlet was 53% at a flow rate of 25 μl/hr. This decreased separation efficiency may be due to the increased viscosity of this fluid which contains RBCs, as opposed to PBS. However, the separation efficiency was greatly improved when we increased the ratio of magnetic nanoparticles to bacteria. At the same flow rate, 78% of the *E. coli* bacteria were retrieved through the collection outlet in a single pass when twice the amount of the magnetic particles were utilized (5×10^6 cells/ml; 1.0×10^{10} magnetic nanoparticles/ml) (Table 1).

Discussion

The ability to remove particles, cells or molecules from flowing blood using a low-cost microsystem technology amenable to multiplexing would have immense clinical significance. In the present study, we constructed an on-chip microfluidic-micromagnetic cell separator and demonstrated its effectiveness for continuous cleansing of contaminant bacteria or particulates from biological fluids. The separation efficiency of magnetic entities at the collection outlet ranged from 78 to over 90% at flow rates of 25 to 40 μl/hr. At low bead or cell densities ($\sim 10^7$ beads or *E. coli*/ml), a throughput of more than 80 beads or cells/s was routinely achieved using the micromagnetic separator (Table 1); moreover, when sorting samples with a high cell density ($\sim 10^9$ RBCs/ml), the throughput of the microdevice increased to 10,000 cells/s (Table 1).

We used nanometer-sized (130 nm) magnetic particles to label the bacteria because they bind more efficiently to *E. coli* compared to micrometer-sized magnetic beads with similar surface functionality (results not shown), possibly due to the increased steric hindrance with micrometer-sized magnetic beads. Magnetic nanoparticles also have the potential advantage that they could be used for in-line applications of this technology in the future (e.g., creating a miniaturized device for cleansing blood of biopathogens in septic patients) because they are less likely to occlude small vessels and have longer circulation times than microbeads (Gupta and Wells, 2004).

Both *E. coli* and the magnetic nanoparticles have multiple binding sites available on their surfaces, and thus they are potential crosslinkers and upon mixing, can form large clusters composed of multiple *E. coli* bacteria. Such clusters will have a much larger effective diameter than an individual *E. coli* bacterium bound to magnetic particles and hence, they will exhibit a decreased magnetic deviation distance in the x-direction (see Eq. (1) in Appendix). Increasing the ratio of magnetic nanoparticles to bacteria reduces the formation of such clusters. We found that when we doubled the ratio of magnetic nanoparticles to bacteria, the separation efficiency of *E. coli* from the fluids containing a physiological concentration of RBCs increased from 53 to 78%. This increased separation efficiency may be due to the reduction in both the size and number of *E. coli*-magnetic nanoparticle clusters.

Heterogeneity in the size and magnetic properties of magnetic susceptible components in the source mixture result in a wide distribution of magnetic deviation distances in the

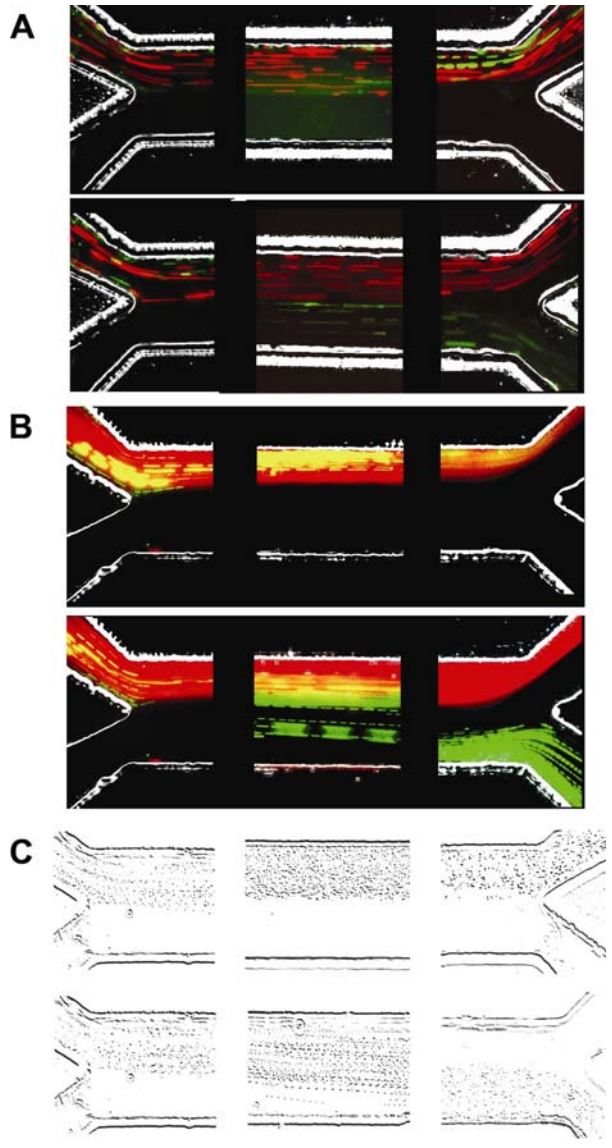

Fig. 4 Magnetic separations using the combined microfluidic-micromagnetic separator with the NiFe microcomb. (A) Red fluorescent non-magnetic beads mixed with green fluorescent magnetic beads in PBS. (B) Green fluorescent magnetic beads mixed with red fluorescent RBCs in saline. (C) *E. coli* cells mixed with magnetic nanoparticles in PBS. Composite fluorescence and bright field images were generated by overlaying sequential frames of corresponding movies taken at the beginning, middle and end (left to right) of the channel, in the presence or absence of the neodymium disk magnet (bottom and top of each pair of images, respectively)

x-direction during continuous separation (see Appendix). Although this is beneficial for applications such as on-chip magnetophoresis (Pamme and Manz, 2004), for magnetic separations of bacteria or cells from biological fluids, variations in magnetic deviation distance needs to be minimized. We used a viscous dextran solution as the collection medium for this purpose (see Eq. (4) in Appendix). Although we occasionally observed sample trapping on the collection side of the channel wall, this effect was small, as indicated by the less than a 10% difference between the separation efficiencies of the magnetic beads and cells calculated with two methods in Table 1 (see footnote c in Table 1).

In our device, the NiFe layer is positioned outside the microfluidic channel to eliminate concerns for the biocompatability of the magnetic materials used. For example, the nickel used in past magnetic separation applications (Han and Frazier, 2004, 2006) can exhibit biocompatibility problems (Takamura et al., 1994; Uo et al., 1999; Wataha et al., 2001). Also, by placing the NiFe layer at a distance (100 μm) from the channel, magnetic particles are less likely to be trapped by the magnetic field at the channel edge. The magnetic field gradient created was found to be effective at driving movement of magnetic microbeads or *E. coli* labeled with magnetic nanoparticles into the collection flow while not significantly displacing RBCs that may be slightly magnetic because they contain deoxyhemoglobin (Melville et al., 1975b; Takayasu et al., 1982) (see Appendix). Finally, to ensure that the magnetic particles flowing at different heights through the channel were exposed to similar magnetic field gradients, we made the thickness of the NiFe magnetic layer equal to the height of the microfluidic channel. Channel height does not affect the separation efficiency of our system, but it influences the volume flow rate. We chose a relatively small channel height (50 μm) to facilitate real-time focusing and monitoring of flows in the channel under microscopic visualization. It should be possible to obtain higher volume throughput by increasing the channel height and the magnetic layer thickness in parallel.

Fluorescence-activated cell sorting (FACS) is another widely used cell separation technology, and on chip FACS devices have achieved a sorting rate of about 100 cells/s (Wang et al., 2005). But because FACS is a serial process allowing only one cell to pass through the actuator at a time, further increases in sample throughput require improvement in the cycle time of the actuator. In contrast, the throughput of our micromagnetic separator increases when the cell density of the sample is raised, and a cell throughput of 10,000 cell/s was demonstrated in the present study. This enhanced throughput is possible because the wide source path used here (1/3–1/2 of channel width) allows large numbers of beads and cells to pass through the separating magnetic field gradient simultaneously. Thus, our design should be especially useful for separations from blood or other clinical samples with high cell density and low optical transparency.

We used a soft magnetic material (NiFe) with low remnant magnetization that was magnetized with an external stationary magnet in this study to facilitate rapid and switchable control of cell separations. Similar systems could also be microfabricated using permanent magnetic materials or that incorporate elements that provide electromagnetic control. Moreover, the same microfabrication techniques could be

used to deposit multiple magnetic layers at different positions on one chip simultaneously; thus multiplexing of the current system is possible in the future.

Appendix: On-chip HGMC-microfluidic design analysis and development

Design analysis

The force on a magnetic particle aligned with a magnetic field is given by $\vec{F}_{\text{mag}} = m\hat{B} \cdot \nabla\vec{B}$, where m is the magnetic moment of the particle, B is the magnetic field, and $\hat{B}$ is the unit vector in the direction of B. In a microfluidic channel with fluid flow in the y-direction and a perpendicular magnetic field gradient in the x-direction, magnetic particles in the fluid will shift toward the maximum of the magnetic field, and traverse the channel in the x-direction (Fig. 1 inset). After passing through the magnetic field, the particle's final distance from the source flow side of channel wall (upper channel edge in Fig. 1 inset) X_{final} is approximated by

$$X_{\text{final}} = \frac{\left(m\frac{d\vec{B}}{dx} \cdot \hat{B}\right)L_y}{3\pi\eta D v_y} + X_{\text{initial}} \tag{1}$$

assuming that (1) the magnetic field gradient is constant across the width of the channel in the x-direction, (2) the magnetic field is constant across the height of the channel in the z-direction, (3) the magnetic force in the y-direction is much smaller than the Stokes drag on the particle, and (4) the source flow and collection flow have similar fluid viscosity η. In Eq. (1), X_{initial} is the distance of the particle from the source flow side of channel wall before entering the magnetic field, D is the particle's effective diameter, L_y is the span of the magnetic field in the y-direction, and v_y is the particle's flow velocity in the y-direction.

It is crucial to maximize the separation efficiency of magnetic particles, i.e. the percentage of magnetic particles that are moved into the collection flow path during passage through the HGMC of the microfluidic channel. On the other hand, it is of equal importance to minimize the loss of the non-magnetic particles from the source flow, i.e. to minimize the percentage of non-magnetic particles that move into the collection flow path during the experiment). In our applications, there are two possible causes for this loss: diffusion and the native magnetic susceptibility of a few cell types, e.g. RBCs containing deoxyhemoglobin.

Diffusion in our system is determined by $d = \sqrt{D_1 L/\bar{v}}$, where D_1 is the diffusion coefficient, d is the diffusion distance, L is the channel length, and $\bar{v}$ is the average flow rate. Diffusion is undesirable for our applications due to the possible loss of critical biomolecules or cells from biological fluids (e.g. blood proteins, platelets). The diffusion coefficients of the smaller proteins are on the order of 10 μm^2/s in water, and they are even smaller in more viscous medium. Assuming $D_1 = 30\,\mu\text{m}^2$/s and the acceptable diffusion distance as 10% of the channel width, it was inferred that the maximum time a fluid volume element should be in the channel is $L/\bar{v} \leq 3.3 \times 10^8 \frac{\text{s}}{\text{m}^2} \cdot W^2$, in which W is channel width. Furthermore, by setting $L_y = kL$ $(0 < k < 1)$ and $v_y \approx \bar{v}$, Eq. (1) is converted to

$$X_{\text{final}} \leq \frac{3.3 \times 10^8\, k \left(m\frac{d\vec{B}}{dx} \cdot \hat{B}\right) W^2}{3\pi\eta D} \quad \text{m} \tag{2}$$

It has been reported (Melville et al., 1975b; Takayasu et al., 1982) that the RBCs containing deoxyhemoglobin have a relative magnetic susceptibility in water (or plasma) of about 3.9×10^{-6}. To prevent the loss of RBCs from the source flow in our system, we set the acceptable deviation of deoxyhemoglobin RBCs in the x-direction after passing through the mangetic field $(X_{\text{final,RBC}} - X_{\text{initial,RBC}})$ as 1/100 of the channel width, W/100.

Design development

For a magnetic particle at given flow conditions, Eq. (1) indicates that X_{final} is a function of m and $\frac{d\vec{B}}{dx} \cdot \hat{B}$. When a magnetic particle is unsaturated $\vec{m} = \chi V\vec{B}/\mu_0$, where χ is the magnetic permeability of the particle, V is the volume of the particle, and μ_0 is the magnetic permeability of vacuum. As B increases, m approaches a saturation value m_s. For convenience, we name the value of $m_s\mu_0/\chi V$ the saturation magnetic field of the particle B_s.

The majority of bioorganisms are non-magnetic, and need to be labeled with superparamagnetic particles in order to be separated from the source mixture. In the present study, the superparamagnetic particles used to label *E. coli* are 130 nm in diameter, and have a magnetic permeability $\chi_{\text{bead}} = 12$ with B_s of 0.02 T. Assuming $\eta = 10^{-3}$ Pa · s (water at 20°C), $D = 3 \times 10^{-6}$ m (*E. coli*) and $B > B_s$, it was inferred from Eq. (2) that to separate *E. coli* bound to a number n of the superparamagnetic particles from the source mixture, $\frac{d\vec{B}}{dx} \cdot \hat{B} > 0.2/knW$ T/m. Based on their size, we estimated that an *E. coli* cell surface can accommodate over 800 of such superparamagnetic particle. If we set the cut-off value for n as 40 (i.e. our system needs to remove *E. coli* bound to at least 40 superparamagnetic particles from the source mixture), $\frac{d\vec{B}}{dx} \cdot \hat{B}$ should be at least $5.0 \times 10^{-3}/kW$ T/m.

In our design, B and $\frac{d\vec{B}}{dx} \cdot \hat{B}$ inside the channel are determined by the magnetic properties, geometry and position

of the HGMC magnetic layer and the external magnetic field. Multiple types of magnetic materials could be used to fabricate the magnetic layer. In the present study, we chose a soft magnetic material (NiFe) with low remnant magnetization that was magnetized with an external stationary magnet to facilitate rapid and switchable control of separations. The NiFe layer has a saturation magnetization ~0.6T (Rasmussen et al., 2001).

Two NiFe layer geometries were tested in the present studies, a microneedle (Fig. 2) and a microcomb (Fig. 3). The microneedle geometry was expected to concentrate magnetic field at one position along the channel and served as a proof of principle for our fabrication technology and manipulation strategy. The microcomb geometry was expected to provide a field gradient along a longer stretch of channel, exposing magnetic particles to force for a longer duration. The magnetic field and field gradient generated by the two NiFe layer geometries were determined by finite element simulations with Maxwell 3D (Ansoft), which solved for magnetic field on a mesh of tetrahedrons that matched the actual device geometry and included the B-H curve of the NiFe layer and the permanent magnet (Figs. 2 and 3).

In our device, the NiFe layer was positioned outside the microfluidic channel to eliminate concerns for the biocompatability of the magnetic materials used. Figure 3 indicates that both B and $\frac{d\vec{B}}{dx} \cdot \hat{B}$ depend on the distance between the magnetic layer and the channel. We determined previously that $\frac{d\vec{B}}{dx} \cdot \hat{B}$ should be at least $5.0 \times 10^{-3}/kW$ T/m, in which k corresponds to the ratio between the span of the magnetic layer in the y-direction L_y and the channel length L. We set k as 0.6 for the microcomb type of magnetic layer to ensure accuracy in device assembly, and the channel width W as 200 μm. Since $\frac{d\vec{B}}{dx} \cdot \hat{B}$ needs to be larger than $5.0 \times 10^{-3}/kW = 42$ T/m, we set the distance between the layer edge and the collection flow side of channel wall as 100 μm. Based on Fig. 3, $\frac{d\vec{B}}{dx} \cdot \hat{B}$ inside the channel is ~55–250 T/m with $0.017\,\text{T} < B_z < 0.02\,\text{T}$ and $0.024\,\text{T} < B_x < 0.048$ T. It was further calculated that assuming $D_{\text{RBC}} = 7\mu$m, and $\chi_{RBC} = 3.9 \times 10^{-6}(X_{\text{final,RBC}} - X_{\text{initial,RBC}})$ is less than 0.1 μm, and less than 1/100 of the channel width, confirming that the loss of RBCs from source flow after passing through the magnetic field is negligible.

Finally, for magnetic separations of *E. coli* (and other bioorganisms or cells as well), the magnetic susceptible entities in the source mixture include both *E. coli* bound to a wide range number of superparamangetic particles and the superparamagnetic particles themselves; this heterogeneity leads to large variations in X_{final}. To minimize such variations as $(X_{\text{final,max}} - X_{\text{final,min}})/W$, we used media with higher fluid viscosity η_c in the collection path than in the source flow path (η_s). By setting $\eta_c = p\eta_s (p > 1)$, Eq. (1) is re-written as

$$X_{\text{final}} = \begin{cases} \dfrac{(m\hat{B} \cdot \nabla \vec{B})L_y}{3\pi\eta D v_y} + X_{\text{initial}}, \\ \quad \text{when } \dfrac{(m\hat{B} \cdot \nabla \vec{B})L_y}{3\pi\eta D v_y} + X_{\text{initial}} \le \dfrac{W}{2} \\ \dfrac{(m\hat{B} \cdot \nabla \vec{B})L_y}{3\pi\eta\, pD v_y} + \dfrac{X_{\text{initial}}}{p} + \dfrac{(p-1)W}{2p}, \\ \quad \text{when } \dfrac{(m\hat{B} \cdot \nabla \vec{B})L_y}{3\pi\eta D v_y} + X_{\text{initial}} > \dfrac{W}{2} \end{cases} \tag{3}$$

Comparing the variations in X_{final} when media with fluid viscosity of η_s and η_c are used in the collection flow respectively, and when both $X_{\text{final,max}}$ and $X_{\text{final,min}}$ are larger than $W/2$, Eq. (3) gives

$$\frac{(X_{\text{final,max}} - X_{\text{final,min}})_{\eta_c}}{(X_{\text{final,max}} - X_{\text{final,min}})_{\eta_s}} = \frac{1}{p} < 1 \tag{4}$$

Hence, using more viscous media in the collection flow can reduce the variations in X_{final}. In experiments, we used a dextran solution, which is both viscous and biocompatible, as the fluid medium for the collection path.

Acknowledgment This work was supported by grants from DOD (DURINT-N000140110782), DARPA (N000140210780), Philip Morris graduate fellowship (to T.P.H.), and NSF to the MRSEC (DMR-0213805) and NRSEC (PHY-0117795) of Harvard University.

References

C.H. Ahn, M.G. Allen, W. Trimmer, Y.N. Jun, and S. Erramilli, J. Microelectromech. S **5**, 151 (1996).
M. Berger, J. Castelino, R. Huang, M. Shah, and R.H. Austin, Electrophoresis **22**, 3883 (2001).
G. Blankenstein, in Microfabricated Flow System for Magnetic Cell and Particle Separation, edited by U. Hafeli, W. Schutt, J. Teller, and M. Zborowski (Plenum Press, New York, 1997), p. 233.
J.J. Chalmers, M. Zborowski, L.P. Sun, and L. Moore, Biotechnol. Progr. **14**, 141 (1998).
B.S. Cho, T.G. Schuster, X. Zhu, D. Chang, G.D. Smith, and S. Takayama, Anal. Chem. **75**, 1671 (2003).
T. Deng, M. Prentiss, and G.M. Whitesides, Appl. Phys. Lett. **80**, 461 (2002).
S. Fiedler, S.G. Shirley, T. Schnelle, and G. Fuhr, Anal. Chem. **70**, 1909 (1998).
M. Franzreb, M. Siemann-Herzberg, T.J. Hobley, and O.R. Thomas, Appl. Microbiol. Biotechnol. (2006).
A.Y. Fu, C. Spence, A. Scherer, F.H. Arnold, and S.R. Quake, Nat. Biotechnol. **17**, 1109 (1999).
C.B. Fuh, and S.Y. Chen, J. Chromatogr. A **813**, 313 (1998).
A.K. Gupta and S. Wells, IEEE Trans. Nanobiosci. **3**, 66 (2004).
K.H. Han and A.B. Frazier, J. Appl. Phys. **96**, 5797 (2004).
K.H. Han and A.B. Frazier, Lab on a Chip **6**, 265 (2006).

R. Handgretinger, P. Lang, M. Schumm, G. Taylor, S. Neu, E. Koscielnak, D. Niethammer, and T. Klingebiel, Bone Marrow Transpl. **21**, 987 (1998).
R. Hartig, M. Hausmann, G. Luers, M. Kraus, G. Weber, and C. Cremer, Rev. Sci. Ins. Trum. **66**, 3289 (1995).
B.L. Hirschbein, D.W. Brown, and G.M. Whitesides, Chemtech **12**, 172 (1982).
L.R. Huang, E.C. Cox, R.H. Austin, and J.C. Sturm, Science **304**, 987 (2004).
T.P. Hunt, H. Lee, and R.M. Westervelt, Appl. Phys. Lett. **85**, 6421 (2004).
D.W. Inglis, R. Riehn, R.H. Austin, and J.C. Sturm, Appl. Phys. Lett. **85**, 5093 (2004).
K.S. Kim, and J.K. Park, Lab on a Chip **5**, 657 (2005).
H. Lee, A.M. Purdon, and R.M. Westervelt, Appl. Phys. Lett. **85**, 1063 (2004).
H. Lu, S. Gaudet, M.A. Schmidt, and K.F. Jensen, Anal. Chem. **76**, 5705 (2004).
J.C. McDonald and G.M. Whitesides, Accounts Chem. Res. **35**, 491 (2002).
D. Melville, F. Paul, and S. Roath, Nature **255**, 706 (1975a).
D. Melville, F. Paul, and S. Roath, IEEE Transactions on Magnetics **11**, 1701 (1975b).
N. Pamme, Lab on a Chip **6**, 24 (2006).
N. Pamme and A. Manz, Anal. Chem. **76**, 7250 (2004).
F.E. Rasmussen, J.T. Ravnkilde, P.T. Tang, O. Hansen, and S. Bouwstra, Sensor Actuat. A-Phys. **92**, 242 (2001).
I. Safarik and M. Safarikova, J Chromatogr B **722**, 33 (1999).
C.H. Setchell, J. Chem. Tech. Biot. B **35**, 175 (1985).
K. Smistrup, B.G. Kjeldsen, J.L. Reimers, M. Dufva, J. Petersen, and M.F. Hansen, Lab on a Chip **5**, 1315 (2005).
K. Takamura, K. Hayashi, N. Ishinishi, T. Yamada, and Y. Sugioka, J. Biomed. Mater. Res. **28**, 583 (1994).
M. Takayasu, N. Duske, S.R. Ash, and F.J. Friedlaender, IEEE Trans. Magnetics **18**, 1520 (1982).
M. Takayasu, D.R. Kelland, and J.V. Minervini, IEEE Trans. Appl. Supercond. **10**, 927 (2000).
A.G.J. Tibbe, B.G. de Grooth, J. Greve, G.J. Dolan, C. Rao, and L. Terstappen, Cytometry **47**, 163 (2002).
M. Uo, F. Watari, A. Yokoyama, H. Matsuno, and T. Kawasaki, Biomaterials **20**, 747 (1999).
M.M. Wang, E. Tu, D.E. Raymond, J.M. Yang, H. Zhang, N. Hagen, B. Dees, E.M. Mercer, A.H. Forster, I. Kariv, P.J. Marchand, and W.F. Butler, Nat. Biotechnol. **23**, 83 (2005).
J.C. Wataha, N.L. O'Dell, B.B. Singh, M. Ghazi, G.M. Whitford, and P.E. Lockwood, J. Biomed. Mater. Res. **58**, 537 (2001).
S. Wolf and R.N. Tauber, Silicon Processing for the VLSI Era, Vol. 1. Process Technology (Lattice Press, 1986).
M. Yamada, M. Nakashima, and M. Seki, Anal. Chem. **76**, 5465 (2004).